Food Chemistry: X 23 (2024) 101775

Contents lists available at ScienceDirect

Food Chemistry: X

journal homepage: www.sciencedirect.com/journal/food-chemistry-x

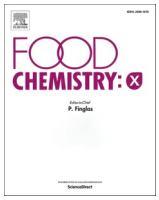

Sweet potato protein hydrolysates solidified calcium-induced alginate gel for enhancing the encapsulation efficiency and long-term stability of purple sweet potato anthocyanins in beads

Mianling Zhang, Yaping Feng, Jianhui Xiao, Chao Sun, Jin Tu, Liya Niu *

School of Food Science and Engineering, Jiangxi Agricultural University, 1101 Zhimin Road, Nanchang 330045, China

ARTICLE INFO

Keywords:
Sodium alginate hydrogel
Gelation behavior
Molecular weight
Bioactive ingredients
Interaction

ABSTRACT

Based on the previous research, this work aimed to reveal the effect of sweet potato protein hydrolysates (SPPHs) with different molecular weights (1000, 3000, and 8000 Da) at 0.5 % on the gelation behavior of calcium-induced sodium alginate (SA), and the encapsulation efficiency and storage stability of purple sweet potato anthocyanins (PSPA) in calcium-induced alginate gel beads was determined. Results indicated that SPPHs with a molecular weight of 8000 Da formed hydrogen bonds and other interactions with SA, which strengthened the internal network connections of the gel, significantly enhanced the gel and effectively filled its pores. The highest encapsulation efficiency was achieved at 87.27 %, compared to 61.73 % without SPPHs. Additionally, stored at 37 °C for 21 days after commercial sterilization, the residual concentration of PSPA with SPPHs was 2.50 times higher than that without SPPHs. SPPHs can enhance the encapsulation efficiency of PSPA and retard their release in gel beads.

1. Introduction

Purple sweet potato anthocyanins (PSPA), which is widely used in the food industry, possess health-promoting benefits of anti-oxidation, hypoglycemia, anti-mutation, liver protection, anti-tumor and anti-inflammation (Li et al., 2019). Nevertheless, PSPA are sensitive to environmental factors such as light, heat and pH, resulting in instability. It has been reported that encapsulation technology could improve the stability of bioactive components by edible carriers to overcome the limitations (Chen, Lin, Chen, & Chiang, 2019).

Sodium alginate (SA) is a polysaccharide consisting α-L-glucuronic acid and β-D-mannuronic acid in a randomized arrangement. Under the induction of calcium ions, it can form a gel network with the structure of an "egg carton" for an effective encapsulation edible carrier to improve the stability of nutrients (Hecht & Srebnik, 2016). However, the aqueous solution of alginate exhibits high viscosity even at low concentrations resulting in a gel network of Ca-alginate with a low density, which leads to the rapid release of the entrapped substance in the environment (Wang, Doi, & Mcclements, 2019). In this regard, other colloids, such as xanthan gum, pectin and carrageenan were used for the solution (Fan, Yang, Duan, & Li, 2021; Zia, Usman, Sabir, Shafiq, & Khan, 2020). Not unexpectedly, the use of colloid compounding results in that colloids are also easy to be thickened and sticky for encapsulation purposes within the leakage of encapsulated nutrients and low long-term stability (Ramdhan, Ching, Prakash, & Bhandari, 2020).

Sweet potato protein hydrolysates (SPPHs) extracted from the by production of sweet potato starch, had antioxidant activity and thermal stability, as well as physiological functions such as lowering blood pressure and lowering blood glucose (Mu, Zhang, & Akinola, 2019). What is more, SPPHs are characterized by high concentration with low viscosity that can increase the solids content in SA gels and achieve high encapsulation efficiency. Additionally, SPPHs with little bitter and relatively balanced amino acid composition, is beneficial for food products in practical applications (Falade, Mu, & Zhang, 2021; Zhang & Mu, 2017). SPPHs as fillers can maintain the structural stability of gluten proteins and improve dough quality(Chen, Xiao, Tu, Yu, & Niu, 2023). Our preliminary study revealed that the SA ionogel exhibited enhanced performance when SPPHs with different molecular weights at 0.25 % were incorporated (Zhang, Xiao, Sun, Feng, & Niu, 2023). The improvement was found to be more pronounced with higher molecular weights of SPPHs. Consequently, it can be hypothesized that an increase in the quantity of SPPHs incorporated into the SA ionogel may result in a more pronounced improvement effect. In order to further validate this hypothesis and apply it to the SA gel encapsulation technique, with the

* Corresponding author.
E-mail address: nly8483@163.com (L. Niu).

https://doi.org/10.1016/j.fochx.2024.101775
Received 10 July 2024; Received in revised form 21 August 2024; Accepted 24 August 2024
Available online 26 August 2024

objective of exploring its improvement effect on the stability of encapsulated PSPA, a further study was conducted. And there was no work that had been carried out to report the effect of SPPHs with different molecular weights as fillers on the encapsulation efficiency and long-term stability of PSPA from alginate beads.

Therefore, the aim of the present work was to investigate the effects of SPPHs with different molecular weights (1000, 3000, and 8000 Da) at 0.5 % on the ionic gelation process of SA. And the interaction between SA and SPPHs was evaluated by ζ-potential and particle size, while alginate-based bead was investigated in terms of encapsulation efficiency, release profiles of PSPA, physicochemical and morphological properties. Additionally, the retention ability and storage stability of PSPA in SA-SPPHs gel beads at pH 4.0 after commercial sterilization also were studied.

2. Materials and methods

2.1. Materials

Sodium alginate (SA) with the mannuronate/guluronate ratio of 1:1 and average molar masse of 1.18 × 10^5 g mol^{-1} was purchased from Qingdao Hai zhi lin Biological Technology Development Co., Ltd. (Qingdao, Shandong, China). Sweet potato protein hydrolysates (SPPHs) with hydrolysis degree of 12 % and molecular weights distribution of 1000–8000 Da were prepared by the method described in our earlier publication (Niu, Wu, & Xiao, 2017). The preparation of purple sweet potato anthocyanins (PSPA) was based on Heinonen's method with some modifications (Jarianssi, Hengameh, & Baoru, 2016). All chemical reagents were of analytical grade and purchased from Xi long Technology Co., Ltd. (Shantou, Guangdong, China).

2.2. Samples preparation

SA at 1 % (*w*/w) and SPPHs with different molecular weights (1000, 3000, and 8000 Da) at 0.5 % (w/w) were weighed and dissolved in distilled water to prepare the SA-SPPHs composite solution. 1.0 % SA solution and 1.5 % SA solution without SPPHs were the blank groups. And the appropriate amount of $CaCl_2$ was dissolved in distilled water into the solutions at 0.050 %, 0.075 %, 0.100 %, 0.125 % and 0.150 %, respectively. For the preparation of the composite gel, the $CaCl_2$ solution was mixed with the SA-SPPHs composite solution at the volume ratio of 2:1.

For the preparation of encapsulated PSPA beads with 0.0 %, 0.2 %, 0.4 % and 0.6 % mass fraction of PSPA, the experimental group was SA at 1.0 % with SPPHs 8000 at 0.5 % and the blank group was SA at 1.5 % configured as the compound cross-linking solutions. The composite cross-linking solutions were dropped into 0.150 % $CaCl_2$ cross-linking solution from a 3 mm diameter mold with continuous stirring for 10 min and then stood for 30 min. The prepared beads were filtered from the cross-linking solution, washed with distilled water for subsequent analysis. The sterilized beads were configured in a preservation solution with a pH of 4 and sterilized at 98 °C for 30 min.

2.3. Particle size and ζ-potential measurements

The particle size and ζ-potentials of different dispersions was determined using dynamic light scattering (Nano ZS, Malvern Instruments Corp., UK) at 25 °C.

2.4. Rheological characterization of SA-SPPHs composite gels

2.4.1. Gelation process measurement

The gelation process of SA-SPPHs composite solutions with calcium ions was measured by time scan mode (DHR-2, TA Instrument Corp., USA). $CaCl_2$ solutions with concentrations of 0.100 %, 0.125 % and 0.150 % were selected to react with the SA-SPPHs composite solution. The test fixture was a 40 mm plate with a 600 μm gap between the test bench and the plate, and the samples were scanned at 80 °C within the linear viscoelastic range for 1200 s (Hu et al., 2022).

2.4.2. Dynamic viscoelasticity measurement

The dynamic viscoelasticity measurement of SA-SPPHs composite gels was performed using a rheometer with a concentric cylinder to determine the variation of storage modulus (G') and loss modulus (G''). The scanning angular frequency was 600.0–0.1 rad/s with 10 % of the strain setting at 25 °C. Each sample was measured for three times, and all samples were tested within the linear viscoelastic range.

2.4.3. Steady-state shear viscosity measurement

The apparent viscosity of the SA-SPPHs composite solutions was measured using a rheometer with a concentric cylinder. The samples were equilibrated for 1 min and then the viscosity was measured in the range of shear rate 0.01–1000 s^{-1}. Each sample was measured for three times.

2.5. Determination of the properties of gel beads

2.5.1. Encapsulation efficiency of PSPA in gel beads

The SA-SPPHs gel beads were prepared and stored at 23 °C for 2 h prior to analysis. The free anthocyanins content (AC) was determined by the pH method. 1 mL of each solution was diluted with pH 1.0 potassium chloride-hydrochloric acid buffer and pH 4.5 sodium acetate buffer, respectively. The absorbance was measured at 527 nm and 700 nm using a UV–visible spectrophotometer (U-T3, Shanghai Yipu Instrument Corp., China), and the content of PSPA was calculated using the formula (1) (Guo, Giusti, & Kaletunç, 2018).

$$AC(\mathrm{mg/L}) = \frac{Ab}{\mathrm{eL}} \times \mathrm{MV} \times \mathrm{D} \times 1000 \quad (1)$$

where $Ab = [(A_{527nm} - A_{700nm})_{\text{pH 1.0}} - (A_{527nm} - A_{700nm})_{\text{pH 4.5}}]$ is, MV, D, e, and L, represents the relative molecular weight of anthocyanin at 449.38 g mol^{-1}, the dilution times, the extinction coefficient of cyanidin-3-*O*-glucoside is 26,900, and the thickness of the cuvette is 1 cm, respectively.

The encapsulation efficiency of PSPA was measured by measuring the AC in the solution and calculated using the formula (2).

$$\text{Encapsulation efficiency}(\%) = \left(1 - \frac{M_1}{M_0}\right) \times 100 \quad (2)$$

where M_0 is the PSPA content initially added in the SA-SPPHs solution, M_1 is the AC in the solution.

2.5.2. Retention rate of PSPA in gel beads

The retention rate of PSPA in gel beads during different storage days were determined by the formula (3).

$$\text{Retention rate}(\%) = \left(1 - \frac{M_3}{M_2}\right) \times 100 \quad (3)$$

where M_2 is the content of PSPA encapsulated in SA-SPPHs gel beads before sterilization, M_3 is the retained PSPA content in beads after sterilization and during the subsequent storage.

2.5.3. Water distribution of gel beads

A 21 MHz low-field nuclear magnetic instrument (Micro MIR-25, Niumag Electronics Technology Corp., China) with a specific pulse sequence was used to calculate the proton transverse relaxation time and diffusion coefficient. The gel beads were equilibrated at 32 °C and placed in a 20 mm glass tube. The sampled data were subjected to single-component inversion to obtain the average relaxation time T_2. And the magnetic resonance imaging (MRI) measurements were obtained using

a multi-slice spin-echo sequence. The resulting image was processed using pseudo-color.

2.5.4. FT-IR of gel beads

The FT-IR spectra of the freeze-dried gel beads were analyzed by a FT-IR spectrometer (Nicolet 5700; Thermo Scientific Nicolet Corp., USA). The spectral scanning range of the samples was 400–4000 cm^{-1} with a resolution of 4 cm^{-1}.

2.5.5. XRD of gel beads

The diffraction spectra of the freeze-dried gel beads were determined by an X-ray diffractometer (XRD-7000, Shimadzu Corp., Japan). The current and voltage were 30 mA and 40 kV, respectively, and the scanning range 2θ was 4–40°.

2.5.6. Microstructure of gel beads

The freeze-dried gel beads visualized at 20× and 100× using a scanning electron microscope (Zeiss evo 18, Carl Zeiss Co., Ltd., Germany) were fixed on a carrier stage and sprayed with gold.

2.5.7. Texture and swelling of gel beads

The hardness and elasticity were measured by texture analyzer with P/0.5 probe for repeated 10 times (TA.TX Plus, Stable Microsystems Ltd., UK). The measurement conditions were as follows: pre-test speed of 1.0 mm/s, test speed of 2.0 mm/s, post-test speed of 2.0 mm/s, compression deformation of 50 %, dwell time of 5 s and trigger force of 5 g. The swelling capacity was expressed by the diameter change of beads.

2.5.8. Storage stability of gel beads

The gel beads encapsulated with PSPA were preserved in a solution at the pH of 4.0 then placed at 37 °C constant temperature for 0, 7, 14 and 21 days for subsequent analysis.

2.6. Statistical analysis

All measurements for samples were conducted in triplicate unless mentioned specially. The data were statistically analyzed by SPSS 26 software. Mean and standard deviation were calculated from three replicates ($n = 3$). Duncan multiple comparison was used for significant difference analysis at $P<0.05$. The graphs were made by Origin 2021 software. Pseudo-color processing of magnetic resonance imaging results used by the MATLAB R2022a software.

3. Results and discussion

3.1. Particle size and ζ-potential analysis of SA-SPPHs composite solutions

As shown in Fig. 1A, the addition of SPPHs with an increased molecular weight produced the increased average particle size of the SA solution, which may be due to the interaction between SPPHs and SA. It had been reported that SA and protein molecules could form complexes via electrostatic repulsion and hydrophobic interactions in a neutral pH environment (Zhao, Zou, Sun, & Yu, 2020). From this, it can be the formation of complexes between SPPHs and SA through the interaction that SPPHs did the increased electrostatic repulsion and the internal structure of the expanded particles. The strength of the interaction and the tightness of the physical cross-links formed between the SA molecular chains increased with the molecular weight of the added SPPHs (Dodero, Vicini, Alloisio, & Castellano, 2019). Compared to our previous study, we also found that adding the same molecular weight and increasing the addition of SPPHs helped to promote the cross-linking effect of sodium alginate gels (Zhang et al., 2023).

The ζ-potential can evaluate the physical stability of the particulate dispersion system. A higher absolute value of ζ-potential indicates stronger electrostatic repulsion between particles (Niu et al., 2015), resulting in better physical stability. As shown in Fig. 1B, the particle surfaces of the SA and SA-SPPHs solutions were negatively charged, and the absolute value of the ζ-potential of SA-SPPHs solution was larger than that of the SA solution. This indicated that there was an electrostatic interaction between the SPPHs and SA. The incorporation of the SPPHs increased the electrostatic repulsive force of the system, which improved the relative stability in the system. This facilitated the strengthening of the network structure of the SA gel beads, which was conducive to improve the encapsulation efficiency and stability of the SA gel beads.

3.2. Calcium ion gelation process analysis of SA-SPPHs composite solutions

The gelling action of SA-SPPHs composite solutions with different mass fractions of $CaCl_2$ solutions were shown in Fig. 2A_1-C_2. The storage modulus G' value and loss modulus G'' value of the SA-SPPHs composite solution increased as the reaction time increased. There was a rapid and significant increase in the G' value at the beginning of the reaction stage, followed by stabilization. At this point, the G' value was significantly higher than the G'' value. This was due to the transformation of the solution into the gel process. The G' value gradually exceeded the G'' value and continued to increase at a faster rate, which was significantly higher than the G'' value (Yang, Campanella, Hamaker, Zhang, & Gu, 2013). Therefore, the rheological phenomena shown in Fig. 2A_1-C_1 confirmed

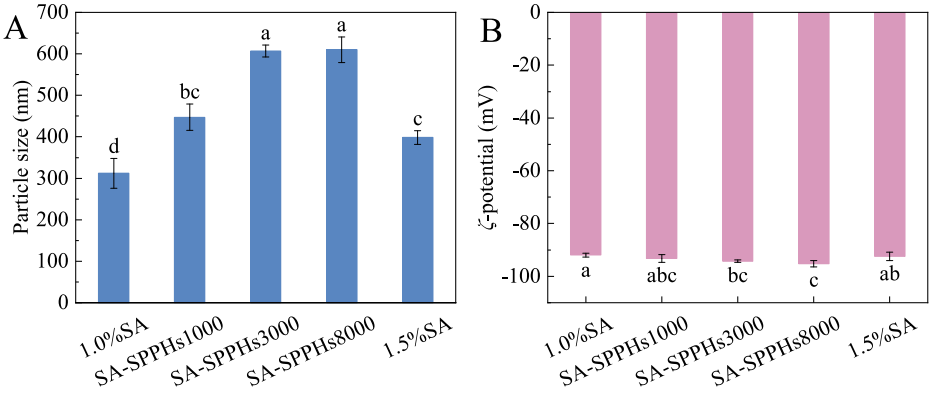

Fig. 1. Particle size (A) and ζ-potential (B) of the complex solution of SA with SPPHs of different molecular weights. (Different letters in the same set of histograms represent significant differences ($P < 0.05$) and same below).

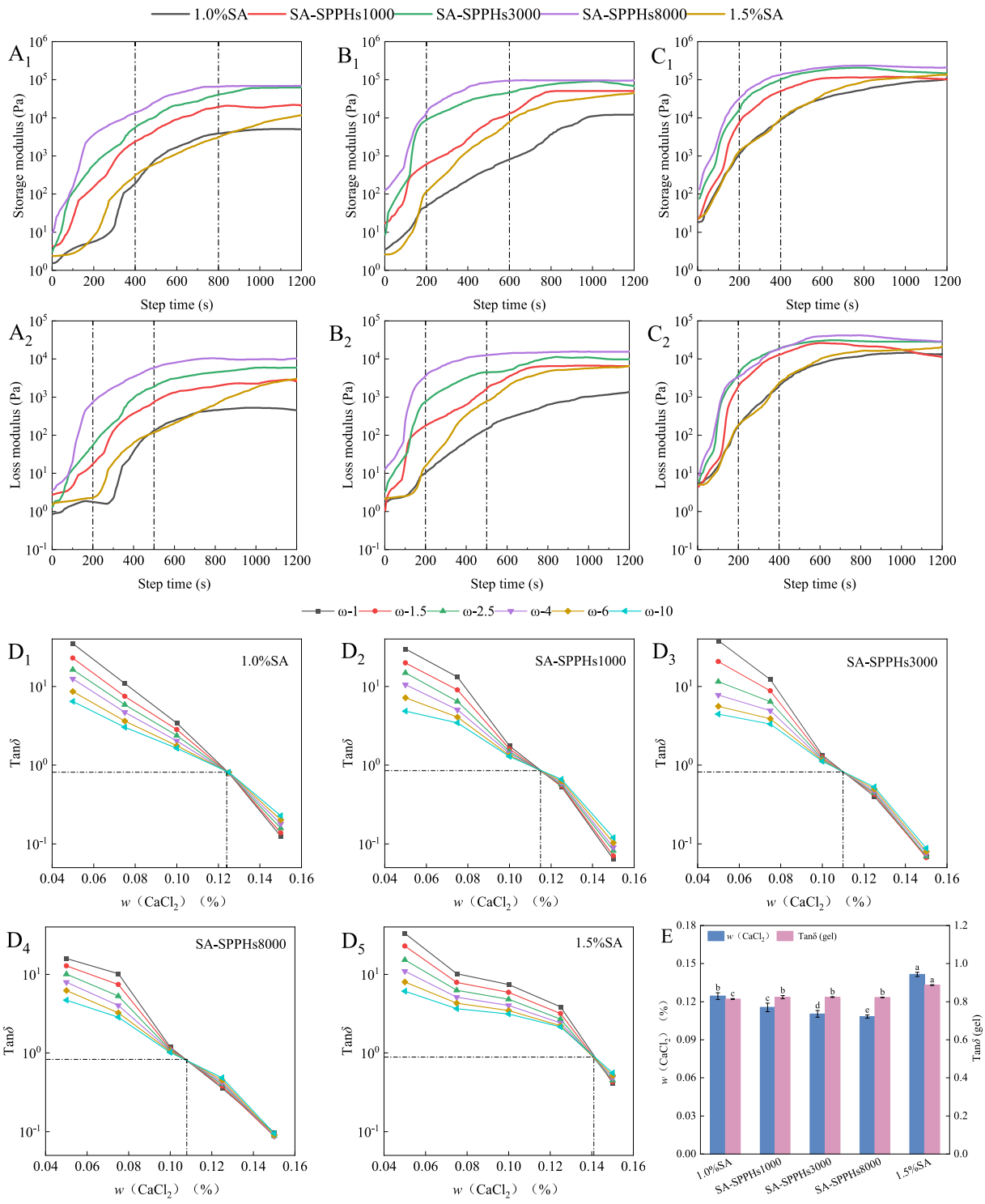

Fig. 2. Gelling analysis of SA-SPPHs solutions with $CaCl_2$ solutions of different mass fractions. 0.100 % $CaCl_2$ (A_1, A_2), 0.125 % $CaCl_2$ (B_1, B_2), 0.150 % $CaCl_2$ (C_1, C_2). Relationship of SA-SPPHs composite gel Tanδ and $CaCl_2$ mass fraction at critical gel point (D_1-D_5). Critical gel parameters of SA-SPPHs composite system (E).

that the gelling process of SA with calcium ions occurred in the SA-SPPHs composite solution with calcium ion system. The addition of SPPHs with different molecular weights resulted in varying degrees of gelling effect. Compared with the blank group of SA, the SA-SPPHs composite solution exhibited greater sensitivity to calcium ion reactions, resulting in a gelling effect and faster stabilization. In Fig. 2A_1, the average values of G' during gelation in descending order were as follows: SA-SPPHs8000 (42.46 kPa), SA-SPPHs3000 (33.02 kPa), SA-SPPHs1000 (13.01 kPa), 1.5 % SA (2.49 kPa) and 1.0 % SA (2.14 kPa). The SPPHs8000 composite solution was the most sensitive with the fastest gelation and the highest strength of gel formation. This further confirmed our previous finding that the effect of calcium gelation was best improved when SPPHs were added at 0.25 %, even when SPPHs were added at a molecular weight of 8000. It was further found that the effect of SPPHs added at 0.50 % was more effective than that of SPPHs added at 0.25 % at the same molecular weight (Zhang et al., 2023).

Fig. 2A_1 showed that the addition of 0.100 % $CaCl_2$ resulted in a

change in G' that can be divided into three regions. When the reaction time was less than 400 s, G' increased rapidly that the gel formation and the development of a three-dimensional network structure may be attributed to the cross-linking between SA-SPPHs and calcium ions. The reaction between SA-SPPHs and calcium ions resulted in differences in the speed and strength of the gel structure reflecting in the changes of G'. The reaction rate of the SA-SPPHs solution with calcium ions was higher than that of the blank group. Additionally, the value of G' was larger, and the modulus size ranged from largest to smallest as SA-SPPHs8000, SA-SPPHs3000, SA-SPPHs1000, and SA. When the reaction time was between 400 s and 800 s, the reaction rate slowed down and the gel was gradually solidified. When the reaction time exceeded 800 s, the gelation process tended to equilibrium. The final equilibrium gel strength of the SA-SPPHs composite solution was greater than that of the SA solution. The increased stability of the gel network structure can be attributed to the calcium ions. The stability of the gel network structure was enhanced by the interaction between SPPHs and SA, which caused intermolecular physical and chemical cross-linking effects, such as hydrogen bonding and molecular chain entanglement (Li, Ma, Chen, He, & Huang, 2018). This interaction increased the internal forces within the functional groups of SA. This interaction contributed to filling the pores of the gel network, which improved the encapsulation efficiency and the stability of the system. The effect was more pronounced with the increase of the molecular weights of the added SPPHs.

As shown in Fig. 2B_1-C_2, the addition of 0.125 % and 0.150 % $CaCl_2$ resulted in a similar pattern of change. The final equilibrium value of G' increased with the calcium ion content, indicating that calcium induced the formation of a more stable gel with a firmer network structure and better interaction between the SPPHs and SA. At equilibrium, G' and G'' remained parallel, demonstrating a typical elastic gel network (Lopes-Da-Silva & Monteiro, 2019).

3.3. Characterization of SA-SPPHs composite gels

3.3.1. Critical gelation behavior

The critical gelation behavior characterized the key point of the reaction between SA-SPPHs composite solution and calcium ions. The size of the critical calcium ion concentration affects the extent of the gel network formation. The relationship between tanδ and $CaCl_2$ mass fraction of the composite gel system measured by small amplitude dynamic rheological scanning was shown in Fig. 2D_1-D_5. Upon the addition of varying mass fractions of $CaCl_2$, the composite gel system's tanδ lost its dependence on the angular frequency at the key gel point and converged at a certain point. Subsequently, the tanδ became independent of the angular frequency, indicating the transformation of the system transformed from a solution to a gel after the critical gel point. As shown in Fig. 2E, the critical calcium ion of mass fraction $CaCl_2$ value decreased with the addition of SPPHs of different molecular weight of SPPHs. The relationship between the molecular weight of SPPHs and the $CaCl_2$ value was inverse, meaning that as the molecular weight increased, the $CaCl_2$ value decreased. Consequently, the amount of calcium ions required for the formation of critical gel sites was also

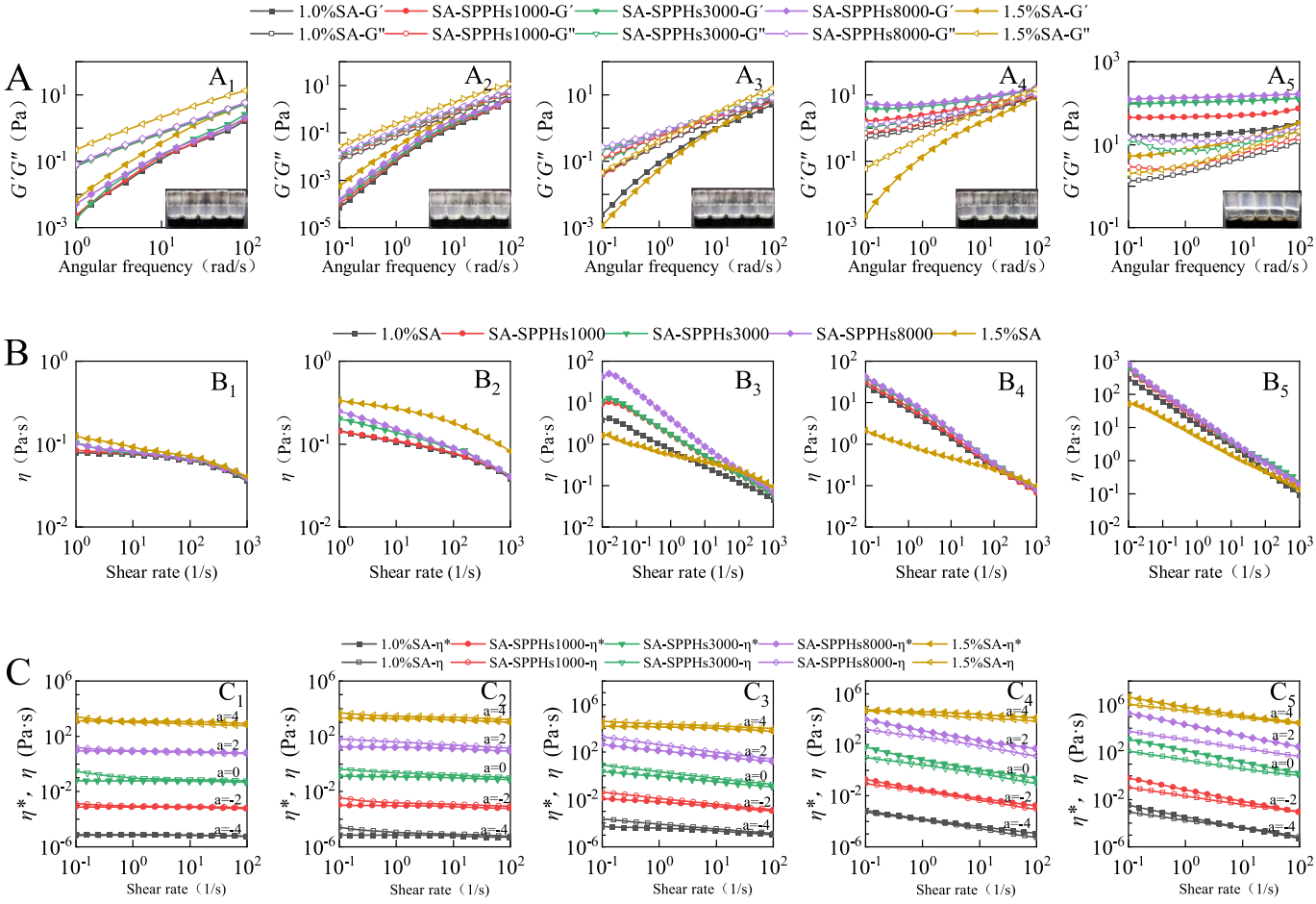

Fig. 3. Dynamic viscoelasticity and visual appearance of SA-SPPHs composite gel (A), Shear viscosity of SA-SPPHs composite gel (B) and comparison of η^* and η of SA-SPPHs composite gel (C) (The data have been shifted by 10^a to avoid overlap, and the value of "a" were indicated in the figure). The mass fractions of $CaCl_2$ solution added were 0.050 % (A_1, B_1, C_1), 0.075 % (A_2, B_2, C_2), 0.100 % (A_3, B_3, C_3), 0.125 % (A_4, B_4, C_4), 0.150 % (A_5, B_5, C_5) respectively. The samples in A_1-A_5 were 1.0 %SA, SA-SPPHs1000, SA-SPPHs3000, SA-SPPHs8000 and 1.5 % SA from left to right.

decreased. The interaction of SPPHs with SA promoted the calcium cross-linking reaction, resulting in the formation of a three-dimensional gel network structure (Li et al., 2018).

3.3.2. Dynamic viscoelastic

Fig. 3A showed the relationship between G' and G'' of the system and the angular frequency with different mass fractions of $CaCl_2$ added to the SA-SPPHs composite solution. The gel strength of the SA-SPPHs composite gel gradually strengthened with the increase of the mass fraction of $CaCl_2$ that shifted from a weak gel-like state to a strong gel state. As the mass fraction of $CaCl_2$ increased, both G' and G'' in the system also increased. This was due to the mutual cross-linking effect of calcium ions and SA, which led to the formation of gels with more cross-linking entanglement points and a tighter three-dimensional network structure that increased G' (Ma, Lin, Chen, Zhao, & Zhang, 2014). Compared with the SA, the G' of the gel with added SPPHs exhibited a higher G' with the modulus in the order of SA-SPPHs8000, SA-SPPHs3000, SA-SPPHs1000, and SA. This may be due to the formation of stronger intermolecular hydrogen bonding between SA and SPPHs with different molecular weights upon the addition of calcium ions, resulting in an increase in the number of cross-linking and entanglement points between SA and calcium ions (Yuan, Wang, Fu, Chang, & Wu, 2022). These findings were consistent with the results of the gelation process. The process of SA crosslinking with calcium ions to form a gel was reacted in Fig. 3A_1-A_5. The addition of 0.050 % and 0.075 % $CaCl_2$ resulted in a gel-like state with $G' < G''$. With the addition of 0.100 % $CaCl_2$, G' tended to converge to G'', resulting in a weakly gel-like state. Finally. With the addition of 0.125 % and 0.150 % $CaCl_2$, $G' > G''$, indicating a stronger solid gel state.

3.3.3. Steady-state shear viscosity

The variation of shear viscosity with shear rate of SA-SPPHs composite solutions with different mass fractions of $CaCl_2$ added was shown in Fig. 3B. The viscosity of SA-SPPHs gels decreased with increasing shear rate that exhibited the phenomenon of “shear thinning". The pseudoplastic fluid property increased with the added of $CaCl_2$. The data points on the shear curves of the composite gels were analyzed using the Power-law rheological model, and the results were shown in Table 1. The data indicated that the value of “n” decreased and the degree of shear thinning and pseudoplasticity increased when the $CaCl_2$ mass fraction was increased from 0.050 % to 0.150 %. Additionally, the degree of pseudoplasticity was found to increase with the molecular weight of the SPPHs added. The SA-SPPHs8000 gel demonstrated the most significant degree of shear thinning and strong pseudoplasticity. This due to the cross-linking of SPPHs and SA through intermolecular van der Waals forces, and hydrogen bonding, which increased the viscosity of the system (Zhao et al., 2020). And the higher the molecular mass weight was, the higher the cross-linking strength was.

In order to further analyze the effect of the interaction between SPPHs and SA, the steady-state shear viscosities of SA-SPPHs compound solutions reacting with different mass fractions of $CaCl_2$ was compared. The Cox-Merz criterion suggested that the composite viscosity η^* and the shear viscosity η were equivalent (Vernon-Carter, Avila-De La Rosa, Carrillo-Navas, Carrera, & Alvarez-Ramirez, 2016). As shown in Fig. 3C, the η^* and η were almost identical when a mass fraction of 0.050 % $CaCl_2$ was added, indicating that the gel forming complied with the Cox-Merz criterion at this point. When $CaCl_2$ was added at mass fractions of 0.075 %, 0.100 %, and 0.125 %, η^* was greater than η in the SA-SPPHs1000, SA-SPPHs3000, and SA-SPPHs8000 systems, while η^* and η were almost identical in the SA systems. When $CaCl_2$ with a mass fraction of 0.150 % added, η^* was greater than η in all the composite systems. The spacing between η^* and η followed a descending order of SA-SPPHs8000, SA-SPPHs3000, SA-SPPHs1000 and SA. The shift in the Cox-Merz criterion indicated the generation of new structure in the system (Zheng, Zeng, Zhang, & Kan, 2019). This had also been supported by the results of the particle size in analysis 3.1. Moreover, the greater the molecular mass of the added SPPHs was, the stronger the interaction was. This resulted in an enhancement of cross-linking within the composite gel and an increase in viscosity.

3.4. Determination of the properties of composite-encapsulated gel beads

3.4.1. Encapsulation efficiency of PSPA

Fig. 4A showed the encapsulation efficiency of the gel beads with PSPA. The encapsulation efficiency of SA-SPPHs gel beads was significantly higher than that of SA gel beads. The highest encapsulation efficiency was achieved with a PSPA addition of 0.6 %, resulting in 61.73 % for SA gel beads and 87.27 % for SA-SPPHs gel beads. The study found that the majority of PSPA were successfully encapsulated in the beads. The encapsulation efficiency was significantly improved by the SPPHs. This improvement may be attributed the interaction between SPPHs and SA, which promoted the cross-linking of SA and calcium ions to form better network connections，and this, in turn effectively filled the pores of the gel network for densing the surface. Consequently, diffusion leakage of the water-soluble PSPA from the surface holes was prevented. Other researches achieve encapsulation by increasing the viscosity of the SA gel structure through the incorporation of filler substances(Lozano-Vazquez et al., 2015). The distinction between this work and previous research is that the interaction of SPPHs with SA facilitated the formation of a gel, which resulted in the construction of a stable network structure. This method of encapsulation is more stable. The addition of PSPA increased the encapsulation efficiency, suggesting that it strengthened the solid barrier of the gels and hindered diffusive transport from the gel interior to the surface. These findings were consistent with our previous results (Liu et al., 2022). Moreover, the high content of SPPHs with the high abundance of alkyl side chains in amino acid residues resulted in the preferential binding of the side-chain groups in SPPHs to the phenolic hydroxyl groups in PSPA (Yin et al., 2021). This interaction improved the stability of PSPA in the gel network, thereby enhancing its encapsulation efficiency.

3.4.2. Water distribution

As shown in Fig. 4B and C, the relaxation time T_2 of SA and SA-SPPHs gel beads with different PSPA additions before (B) and after (C) sterilization were determined. The T_2 reflects the strength of the interaction between water and other substances. Compared with SA gel beads, the T_2 values of SA-SPPHs gel beads were significantly reduced. This suggested the intermolecular interactions were enhanced, resulting in a

Table 1
Power-law equation fitting parameters of SA-SPPHs composite gel.

Sample	0.050 %$CaCl_2$			0.075 %$CaCl_2$			0.100 %$CaCl_2$			0.125 %$CaCl_2$			0.150 %$CaCl_2$		
	k	n	R^2	k	n	R^2	k	n	R^2	k	n	R^2	k	n	R^2
1.0 %SA	0.086	0.916	0.996	0.103	0.731	0.999	0.843	0.635	0.998	8.117	0.463	0.999	13.083	0.317	0.999
SA-SPPHs1000	0.090	0.915	0.997	0.136	0.700	0.998	2.165	0.628	0.998	8.751	0.415	0.997	13.741	0.184	0.999
SA-SPPHs3000	0.101	0.892	0.997	0.204	0.543	0.997	3.170	0.599	0.998	10.479	0.410	0.996	17.574	0.119	0.999
SA-SPPHs8000	0.102	0.891	0.997	0.248	0.433	0.997	6.604	0.545	0.996	10.654	0.390	0.997	17.757	0.080	0.998
1.5 %SA	0.126	0.862	0.999	0.344	0.685	0.998	0.583	0.772	0.998	0.949	0.639	0.997	7.133	0.546	0.999

Different letters in the same column indicated significant differences ($P < 0.05$).

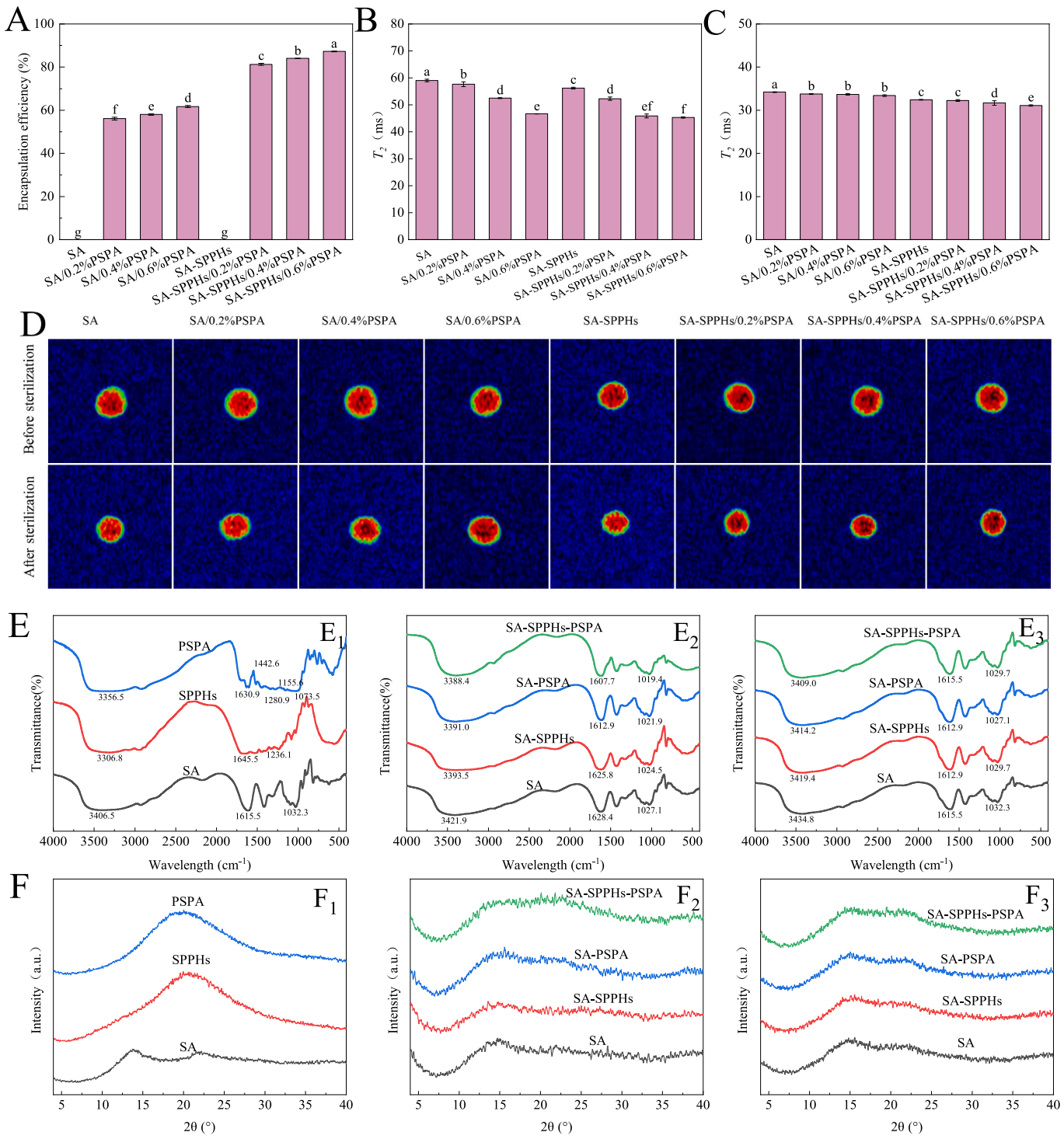

Fig. 4. Encapsulation efficiency of PSPA in gel beads (A), Relaxation time (T_2) before (B) and after (C)sterilization of gel beads with different PSPA additions, Pseudo-color map of proton distribution of SA and SA-SPPHs gel beads with different PSPA additions (D), FT-IR (E) and XRD (F) (where the samples were raw materials (E_1, F_1); SA, SA-SPPHs gel beads and PSPA-embedded gel beads before (E_2, F_2) and after (E_3, F_3) sterilization).

reduction the freedom of water. Furthermore, the addition of PSPA decreased the T_2 values. The study found that SPPHs significantly impacted the water state of the gel beads. Additionally, the PSPA resulted in a more stable water state that was bound within the gel structure. This was due to the formation of hydrogen bonds between the amino groups in specific amino acid peptides of the SPPHs and the hydroxyl group of the water molecules. As a result, the freedom of water was reduced. The findings of Chen et al. (Chen, Wu, Cai, & Wang, 2021) were consistent with this result. The PSPA caused a change in solidification within the gel beads.

Fig. 4D showed the results obtained by MRI measurements for revealing the enhancement of hydrogen proton signals in the samples. The colors blue, green, red and black appeared sequentially in the image with the intensity of hydrogen protons gradually increasing from the outer to the inner regions. The SA-SPPHs gel beads had smaller external blue-green areas and more uniform and concentrated internal black areas. In all the pseudo-color images of the samples, it is evident that the SA-SPPHs/0.6 % PSPA gel beads displayed the largest black and the

narrowest blue area. This suggested that there were sufficient free hydrogen proton signals in this area (Wang et al., 2021). The PSPA trapped the water in the gel network, forming the gel with a denser three-dimensional structure.

3.4.3. FT-IR analysis

FT-IR spectroscopy was used to analyze the structural characterization and stability of SA and SA-SPPHs gel beads with/without PSPA before (E_2) and after (E_3) sterilization. The infrared spectra of SA-PSPA gel beads and SA-SPPHs-PSPA gel beads exhibited similar patterns to PSPA , such as the aromatic ring C═C stretching vibration at 1442.6 cm^{-1}, the aromatic ring C-O-C stretching vibration at 1073.5 cm^{-1}, and the phenol C—O angular deformation at 1280.9 cm^{-1}. The results showed successful encapsulation of PSPA in both SA and SA-SPPHs gels. The SPPHs resulted in a shift of the intermolecular hydrogen bonding absorption peak from 3391.0 cm^{-1} to 3388.4 cm^{-1}, indicating an increased number of hydrogen bonds between SA and SPPHs and stronger interactions within the composite system (Liu et al., 2022). A more compact three-dimensional network structure formed within the gel improved its encapsulation stability. The absorption peaks of hydrogen bonding in the bead patterns of the PSPA-added gels were also shifted to lower wave numbers compared with those without PSPA, possibly due to the formation of hydrogen bonding interactions between PSPA and SPPHs. The spectra of the gel beads in Fig. 4E_3 exhibited a similar pattern after sterilization, indicating that the network structure of the composite gels was strengthened by the hydrogen bonding interactions. This enhancement increased gel strength and water retention capacity that was consistent with the results of the water distribution.

3.4.4. XRD analysis

Fig. 4F showed the X-ray diffractograms of SA and SA-SPPHs gel beads with/without PSPA before (F_2) and after sterilization (F_3). All the gel beads exhibited a broader diffraction peak at $2\theta = 14.5°$. However, the diffraction pattern of the SA-SPPHs-PSPA gel beads exhibited a relatively broader diffraction peak at $2\theta = 22.5°$, and the diffraction peaks had an overall broader and weaker shape compared with the SA-PSPA gel beads. The results indicated the SPPHs increased the amorphous region, and there may be electrostatic interactions between PSPA and SPPHs. It had been demonstrated that the presence of amorphous forms enhances intermolecular interactions among different polymers. Hydrogen bonding within the polymers can promote the formation of amorphous regions, leading to interactions between SPPHs and SA (Bajpai, Shukla, & Bajpai, 2016). The strengthening effect of PSPA promoted the stabilization of the internal structure of the SA gel, while its external amorphous region acted to wrap and encapsulate PSPA more effectively. The overall peaks of the post-sterilization profiles of the gel beads showed weaker and less intense overall peaks compared to the pre-sterilization profiles. This change may be attributed to the promotion of more amorphous structures within the gel due to heat treatment, resulting in a firmer and denser internal network structure.

3.4.5. Microstructure analysis

Fig. 5 showed the surface microstructures of SA and SA-SPPHs gel beads with different PSPA additions. The majority of the lyophilized gel beads were in a well spherical in shape with varying degrees of surface wrinkles, possibly caused by ice crystal expansion during lyophilization and polymer collapse (Tsai, Kitamura, & Kokawa, 2017). After sterilization, the surface porosity and roughness of the gel beads decreased, resulting in a smoother surface. This was due to the heat treatment, which rearranged the alginate structure and shortened the distances between the polysaccharide chains. Consequently, a more networked structure made up of hydrogen bonds was formed to the smoother surface (Tsai, Chiang, Kitamura, Kokawa, & Islam, 2017). Compared with SA gel beads, SA-SPPHs gel beads had a smoother surface with fewer surface wrinkles, indicating that the SPPHs resulted in a denser and tighter structure. The SPPHs also induced a change in the microstructure of the gel, which supported the bead structure during the lyophilization process. However, the addition of PSPA resulting in smoother surface morphology of the gel beads with a uniformly dense network structure and improved the encapsulation. Therefore, the addition of SPPHs and PSPA had the reinforcing effect on SA-based gel beads. These findings were consistent with the results of the encapsulation efficiency. With increasing PSPA addition, more PSPA was encapsulated in the gel beads, resulting in a darker color. The gel beads made from SA-SPPHs exhibited a darker color and lower transparency compared to those made solely with SA. This change was due to the interaction between the SPPHs and the PSPA, resulting in the formation of that strengthened the gel structure (Le Bourvellec & Renard, 2012).

3.5. Storage stability of composite-encapsulated gel beads

3.5.1. Retention ability of PSPA

The retention rate of gel beads during storage after sterilization was shown in Fig. 6A. The loose and porous structure of SA gel network

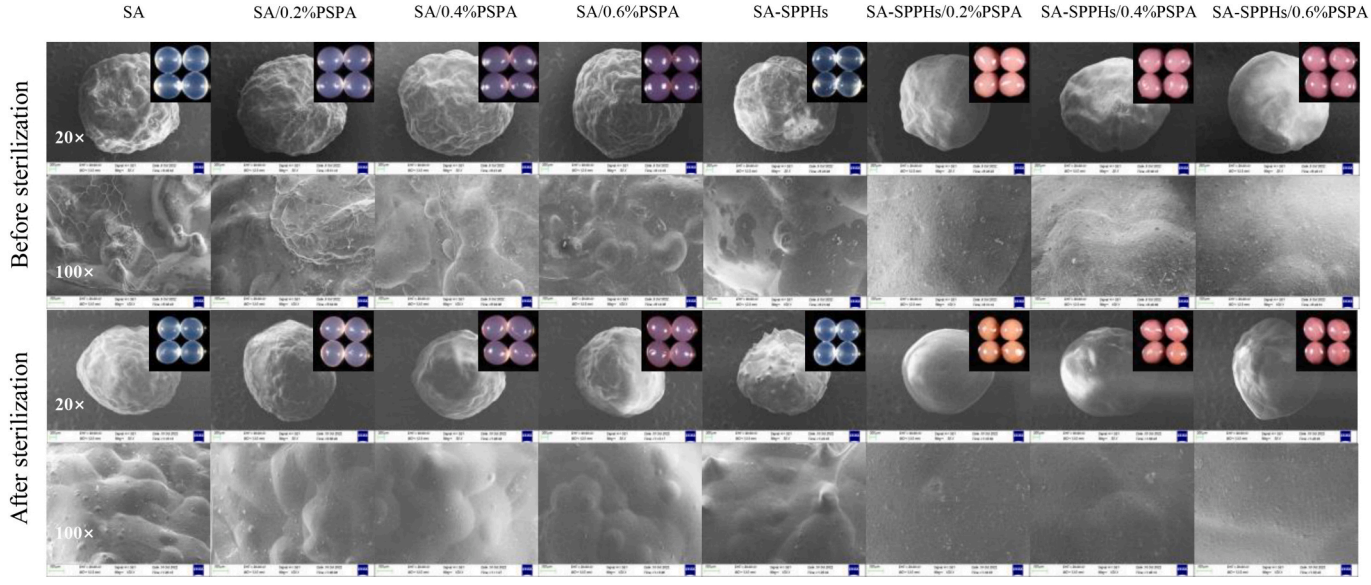

Fig. 5. The visual appearance and surface microstructure of gel beads.

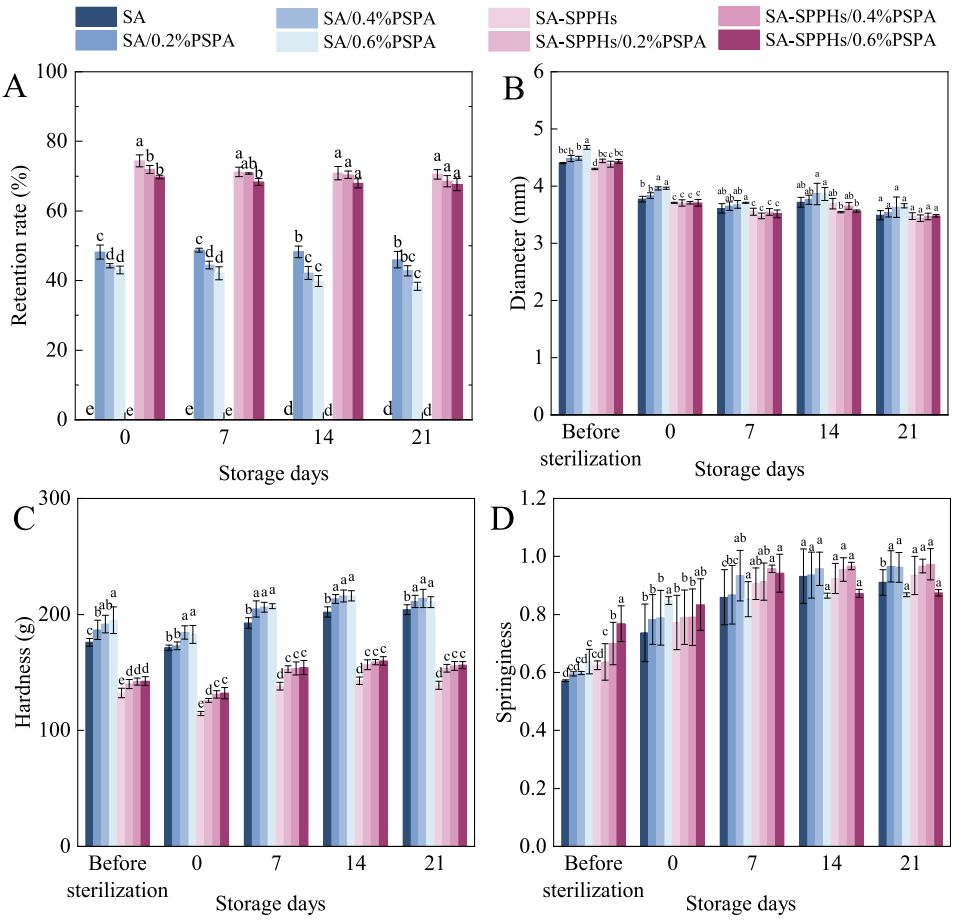

Fig. 6. Retention rate of PSPA in gel beads during storage after sterilization (A); The changes in diameter (B), hardness (C) and springiness (D) of gel beads during storage after sterilization.

caused the leakage of PSPA encapsulated in the gel beads. The retention rate of PSPA in the SA-SPPHs gel beads was 60 %–70 %, significantly higher than that in the SA gel beads (30 %–50 %). This was due to the intrinsic instability of PSPA, which was susceptible to disruption and degradation under heat-treatment conditions in SA gels without SPPHs added. This resulted in the loss of PSPA from the loose and porous SA gel network. The residual concentration of PSPA in gel beads with SPPHs was 2.50 times higher than that without SPPHs. This improved retention rate after sterilization due to strong interactions between SPPHs and PSPA, primarily through hydrogen bonding and hydrophobic interactions, which were not easily disrupted by heat treatment (He et al., 2021). However, increasing the amount of PSPA led to a decrease in retention rate due to PSPA's instability with heat treatment and degradation loss (Jiang & Zhang, 2023). The retention rate remained stable during constant temperature storage, indicating effective encapsulation in the SA-based gel system for PSPA.

3.5.2. Texture and swelling force

As shown in Fig. 6C and D, the textural properties of SA and SA-SPPHs gel beads were improved after sterilization, resulting in increased overall hardness and elasticity. The loss of free water from the gel beads during sterilization led to tighter polymerization within the gel, which improved the textural properties. Research had demonstrated that the rearrangement of alginate chains during gel formation followed by heat treatment, contributed to the development of a more compact gel network structure (Serp, Mueller, Von Stockar, & Marison, 2002). The resulted SA gel beads were firmer, while the SA-SPPHs gel beads were more flexible. Gel formation occurred primarily through cross-linking between SA molecules and calcium ions. The SA gel beads contained a significant amount of SA, resulting in stronger cross-linking and improved structural properties. However, the SPPHs can act as an effective plasticizer to enhance the flexibility of the polymers in the gel beads. This reduced the energy required for molecular movement and the hydrogen bonds formation. The gel beads became easily compressible with higher elasticity properties (Abdin, Salama, Gawad, Fathi, & Alnadari, 2021). After sterilization, the gel beads were shrunk by approximately 10 % due to water loss and rearrangement of the internal gel structure. This resulted in a more uniform and dense network structure. The overall size of the gel beads did not significantly change during long-term storage.

4. Conclusion

The effects of SPPHs with different molecular weights (1000, 3000, and 8000 Da) on the formation of SA gels induced by calcium ions and the encapsulation efficiency and storage stability of PSPA in fabricated calcium-induced sodium alginate beads were analyzed. It was concluded that the interactions of SPPHs with SA promoted its cross-linking with calcium ions, which contributed to the improvement of the gel speed and strength of SA during the process of calcium cross-linking. The strengthening effect was significant for SPPHs with a molecular weight of 8000 Da. It was also found that when the molecular weights of the added SPPHs were the same, increasing the amount of SPPHs added contributed to this strengthening effect. The addition of SPPHs promoted the gelation of SA. The critical gelation point mass fraction of calcium ions decreased with increasing molecular weight of the SPPHs, facilitating the formation of a three-dimensional gel network structure. Additionally, the SPPHs effectively filled the surface pores of the SA gels,

resulting in high encapsulation efficiency and retention rate of the SA gels after sterilization. The optimal encapsulation effect occurred with a PSPA addition of 0.6 %. The SA-SPPHs gel beads exhibited a significantly higher encapsulation efficiency (87.27 %) compared to the SA gel beads (61.73 %). After sterilization at 98 °C with pH 4.0, the residual concentration of PSPA in the gel beads with SPPHs was 2.50 times higher than that without SPPHs when stored at 37 °C for 21 days. The addition of SPPHs improved the textural properties of SA gels and significantly reduced the T_2 value. Hydrogen bonding between SPPHs and SA molecules resulted in a tighter filling of water inside the gels for enhancing the water-holding capacity of the SA gels and providing better storage stability. Furthermore, SPPHs retard its release from the gel beads and applied in the preparation of hydrogel food products with high nutritional value which has potential applications in the food industry.

CRediT authorship contribution statement

Mianling Zhang: Writing – original draft, Methodology, Investigation, Formal analysis, Data curation. **Yaping Feng:** Writing – review & editing, Methodology. **Jianhui Xiao:** Writing – review & editing, Methodology, Funding acquisition. **Chao Sun:** Writing – review & editing. **Jin Tu:** Writing – review & editing. **Liya Niu:** Writing – review & editing, Supervision, Project administration, Funding acquisition, Conceptualization.

Declaration of competing interest

The authors declare that they have no known competing financial interests or personal relationships that could have appeared to influence the work reported in this paper.

Data availability

Data will be made available on request.

Acknowledgments

This research was supported by the National Natural Science Foundation of China (No. 31960458) and the Earmarked Fund for Jiangxi Agriculture Research System (JXARS-19-4).

References

Abdin, M., Salama, M. A., Gawad, R. M. A., Fathi, M. A., & Alnadari, F. (2021). Two-steps of gelation system enhanced the stability of Syzygium cumini anthocyanins by encapsulation with sodium alginate, maltodextrin, chitosan and gum Arabic. *Journal of Polymers and the Environment, 29*(11), 3679–3692. https://doi.org/10.1007/s10924-021-02140-3

Bajpai, M., Shukla, P., & Bajpai, S. K. (2016). Ca(II)+Ba(II) ions crosslinked alginate gels prepared by a novel diffusion through dialysis tube (DTDT) approach and preliminary BSA release study. *Polymer Degradation and Stability, 134*, 22–29. https://doi.org/10.1016/j.polymdegradstab. 2016.09.027

Chen, C., Lin, C., Chen, M., & Chiang, P. (2019). Stability and quality of anthocyanin in purple sweet potato extracts. *Foods, 8*(9), 393. https://doi.org/10.3390/foods8090393

Chen, J., Xiao, J., Tu, J., Yu, L., & Niu, L. (2023). The alleviative effect of sweet potato protein hydrolysates on the qualitydeterioration of frozen dough bread in comparison to trehalose. *LWT, 175*, Article 114505. https://doi.org/10.1016/i.lwt.2023.114505

Chen, X., Wu, J., Cai, X., & Wang, S. (2021). Production, structure–function relationships, mechanisms, and applications of antifreeze peptides. *Comprehensive Reviews in Food Science and Food Safety, 20*(1), 542–562. https://doi.org/10.1111/1541-4337.12655

Dodero, A., Vicini, S., Alloisio, M., & Castellano, M. (2019). Sodium alginate solutions: Correlation between rheological properties and spinnability. *Journal of Materials Science, 54*(10), 8034–8046. https://doi.org/10.1007/s10853-019-03446-3

Falade, E. O., Mu, T., & Zhang, M. (2021). Improvement of ultrasound microwave-assisted enzymatic production and high hydrostatic pressure on emulsifying, rheological and interfacial characteristics of sweet potato protein hydrolysates. *Food Hydrocolloids, 117*, Article 106684. https://doi.org/10.1016/j.foodhyd.2021.106684

Fan, Y., Yang, J., Duan, A., & Li, X. (2021). Pectin/sodium alginate/xanthan gum edible composite films as the fresh-cut package. *International Journal of Biological Macromolecules, 181*, 1003–1009. https://doi.org/10.1016/j.ijbiomac.2021.04.111

Guo, J., Giusti, M. M., & Kaletunç, G. (2018). Encapsulation of purple corn and blueberry extracts in alginate pectin hydrogel particles: Impact of processing and storage parameters on encapsulation efficiency. *Food Research International, 107*, 414–422. https://doi.org/10.1016/j.foodres.2018.02.035

He, W., Yin, Z., Liu, S., Chen, Y., Qie, X., Chen, J., … He, Z. (2021). Effect of preheated milk proteins and bioactive compounds on the stability of cyanidin-3-O-glucoside. *Food Chemistry, 345*, Article 128829. https://doi.org/10.1016/j.foodchem.2020.128829

Hecht, H., & Srebnik, S. (2016). Structural characterization of sodium alginate and calcium alginate. *Biomacromolecules, 17*(6), 2160–2167. https://doi.org/10.1021/acs.biomac.6b00378

Hu, C., Lu, W., Sun, C., Zhao, Y., Zhang, Y., & Fang, Y. (2022). Gelation behavior and mechanism of alginate with calcium: Dependence on monovalent counterions. *Carbohydrate Polymers, 294*, Article 119788. https://doi.org/10.1016/j.carbpol.2022.119788

Jarianssi, H., Hengameh, F., & Baoru, S. V. H. K. (2016). Extraction and purification of anthocyanins from purple-fleshed potato. *Food and Bioproducts Processing, 99*, 136–146. https://doi.org/10.1016/j.fbp.2016.05.004

Jiang, M., & Zhang, Y. (2023). Biopolymer-based encapsulation of anthocyanins as reinforced natural colorants for food applications. *Journal of Agriculture and Food Research, 11*, Article 100488. https://doi.org/10.1016/j.jafr.2022.100488

Le Bourvellec, C., & Renard, C. M. (2012). Interactions between polyphenols and macromolecules: Quantification methods and mechanisms. *Critical Reviews in Food Science and Nutrition, 52*(3), 213–248. https://doi.org/10.1080/10408398.2010.499808

Li, A., Xiao, R., He, S., An, X., He, Y., Wang, C., … He, J. (2019). Research advances of purple sweet potato anthocyanins: Extraction, identification, stability, bioactivity, application, and biotransformation. *Molecules, 24*(21), 3816. https://doi.org/10.3390/molecules24213816

Li, J., Ma, J., Chen, S., He, J., & Huang, Y. (2018). Characterization of calcium alginate/deacetylated konjac glucomannan blend films prepared by Ca^{2+} crosslinking and deacetylation. *Food Hydrocolloids, 82*, 363–369. https://doi.org/10.1016/j.foodhyd.2018.04.022

Liu, L., Zhang, D., Song, X., Guo, M., Wang, Z., Geng, F., … Nie, S. (2022). Compound hydrogels derived from gelatin and gellan gum regulates the release of anthocyanins in simulated digestion. *Food Hydrocolloids, 127*, Article 107487. https://doi.org/10.1016/j.foodhyd.2022.107487

Liu, S., Xiao, J., Feng, Y., Zhang, M., Li, Y., Tu, J., & Niu, L. (2022). Anthocyanin-fortified konjac glucomannan/sodium alginate composite edible boba: characteristics of texture, microstructure,in vitro release behaviour and antioxidant capacity. *International Journal of Food Science & Technology, 57*(3), 1791–1803. https://doi.org/10.1111/ijfs.15557

Lopes-Da-Silva, J. A., & Monteiro, S. R. (2019). Gelling and emulsifying properties of soy protein hydrolysates in the presence of a neutral polysaccharide. *Food Chemistry, 294*, 216–223. https://doi.org/10.1016/j.foodchem.2019.05.039

Lozano-Vazquez, G., Lobato-Calleros, C., Escalona-Buendia, H., Chavez, G., Alvarez-Ramirez, J., & Vernon-Carter, E. J. (2015). Effect of the weight ratio of alginate-modified tapioca starch on the physicochemical properties and release kinetics of chlorogenic acid containing beads. *Food Hydrocolloids, 48*, 301–311. https://doi.org/10.1016/j.foodhyd.2015.02.032

Ma, J., Lin, Y., Chen, X., Zhao, B., & Zhang, J. (2014). Flow behavior, thixotropy and dynamical viscoelasticity of sodium alginate aqueous solutions. *Food Hydrocolloids, 38*, 119–128. https://doi.org/10.1016/j.foodhyd.2013.11.016

Mu, T., Zhang, M., & Akinola, L. (2019). Sweet potato protein and its hydrolysates. *Sweet potato*, 69–115. https://doi.org/10.1016/B978-0-12-813637-9.00004-1

Niu, F., Dong, Y., Shen, F., Wang, J., Liu, Y., Su, Y., … Yang, Y. (2015). Phase separation behavior and structural analysis of ovalbumin–gum arabic complex coacervation. *Food Hydrocolloids, 43*, 1–7. https://doi.org/10.1016/j.foodhyd.2014.02.009

Niu, L., Wu, L., & Xiao, J. (2017). Inhibition of gelatinized rice starch retrogradation by rice bran protein hydrolysates. *Carbohydrate Polymers, 175*, 311–319. https://doi.org/10.1016/j.carbpol.2017.07.070

Ramdhan, T., Ching, S. H., Prakash, S., & Bhandari, B. (2020). Physical and mechanical properties of alginate based composite gels. *Trends in Food Science & Technology, 106*, 150–159. https://doi.org/10.1016/j.tifs.2020.10.002

Serp, D., Mueller, M., Von Stockar, U., & Marison, I. W. (2002). Low-temperature Electron microscopy for the study of polysaccharide Ultrastructures in hydrogels. II. Effect of temperature on the structure of Ca^{2+}-alginate beads. *Biotechnology and Bioengineering, 3*(79), 253–259. https://doi.org/10.1002/bit.10287

Tsai, F., Chiang, P., Kitamura, Y., Kokawa, M., & Islam, M. Z. (2017). Producing liquid-core hydrogel beads by reverse spherification: Effect of secondary gelation on physical properties and release characteristics. *Food Hydrocolloids, 62*, 140–148. https://doi.org/10.1016/j.foodhyd.2016.07.002

Tsai, F. H., Kitamura, Y., & Kokawa, M. (2017). Effect of gum arabic-modified alginate on physicochemical properties, release kinetics, and storage stability of liquid-core hydrogel beads. *Carbohydrate Polymers, 174*, 1069–1077. https://doi.org/10.1016/j.carbpol.2017.07.031

Vernon-Carter, E. J., Avila-De La Rosa, G., Carrillo-Navas, H., Carrera, Y., & Alvarez-Ramirez, J. (2016). Cox-Merz rules from phenomenological Kelvin-Voigt and Maxwell models. *Journal of Food Engineering, 169*, 18–26. https://doi.org/10.1016/j.jfoodeng.2015.08.005

Wang, M., Doi, T., & Mcclements, D. J. (2019). Encapsulation and controlled release of hydrophobic flavors using biopolymer-based microgel delivery systems: Sustained

release of garlic flavor during simulated cooking. *Food Research International, 119*, 6–14. https://doi.org/10.1016/j.foodres.2019.01.042

Wang, Y., Han, Y., Yan, J., Du, Y., Jiang, X., & Wu, H. (2021). Gel properties and network structure of the hydrogel constructed by iota-carrageenan and Ala-Lys dipeptide. *International Journal of Biological Macromolecules, 182*, 244–251. https://doi.org/10.1016/j.ijbiomac.2021.04.001

Yang, Y., Campanella, O. H., Hamaker, B. R., Zhang, G., & Gu, Z. (2013). Rheological investigation of alginate chain interactions induced by concentrating calcium cations. *Food Hydrocolloids, 30*(1), 26–32. https://doi.org/10.1016/j.foodhyd.2012.04.006

Yin, Z., Wu, Y., Chen, Y., Qie, X., Zeng, M., Wang, Z., … He, Z. (2021). Analysis of the interaction between cyanidin-3-O-glucoside and casein hydrolysates and its effect on the antioxidant ability of the complexes. *Food Chemistry, 340*, Article 127915. https://doi.org/10.1016/j.foodchem.2020.127915

Yuan, Y., Wang, H., Fu, Y., Chang, C., & Wu, J. (2022). Sodium alginate/gum arabic/glycerol multicomponent edible films loaded with natamycin: Study on physicochemical, antibacterial, and sweet potatoes preservation properties. *International Journal of Biological Macromolecules, 213*, 1068–1077. https://doi.org/10.1016/j.ijbiomac.2022.06.040

Zhang, M., & Mu, T. H. (2017). Identification and characterization of antioxidant peptides from sweet potato protein hydrolysates by Alcalase under high hydrostatic pressure. *Innovative Food Science & Emerging Technologies, 43*, 92–101. https://doi.org/10.1016/j.ifset.2017.08.001

Zhang, M., Xiao, J., Sun, C., Feng, Y., & Niu, L. (2023). Effects of sweet potato protein hydrolysates on formation of calcium ion-induced sodium alginate gel. *Journal of Food Science and Technology, 41*(4), 67–81. https://doi.org/10.12301/spxb202200861

Zhao, N., Zou, H., Sun, S., & Yu, C. (2020). The interaction between sodium alginate and myofibrillar proteins: The rheological and emulsifying properties of their mixture. *International Journal of Biological Macromolecules, 161*, 1545–1551. https://doi.org/10.1016/j.ijbiomac.2020.08.025

Zheng, J., Zeng, R., Zhang, F., & Kan, J. (2019). Effects of sodium carboxymethyl cellulose on rheological properties and gelation behaviors of sodium alginate induced by calcium ions. *LWT, 103*, 131–138. https://doi.org/10.1016/j.lwt.2018.12.081

Zia, T., Usman, M., Sabir, A., Shafiq, M., & Khan, R. U. (2020). Development of inter-polymeric complex of anionic polysaccharides, alginate/k-carrageenan bio-platform for burn dressing. *International Journal of Biological Macromolecules, 157*, 83–95. https://doi.org/10.1016/j.ijbiomac.2020.04.157